

Pyramidalization of the Glycosidic Nitrogen Provides the Way for Efficient Cleavage of the N-Glycosidic Bond of 8-OxoG with the hOGG1 DNA Repair Protein

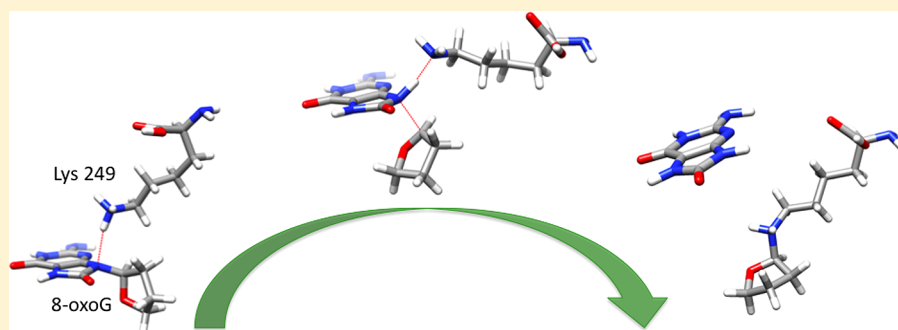
Jakub Šebera,[†] Lukáš Trantírek,[‡] Yoshiyuki Tanaka,[§] and Vladimír Sychrovský^{*,†}

[†]Institute of Organic Chemistry and Biochemistry AS CR, v.v.i., Flemingovo náměstí 2, CZ, 16610 Praha, Czech Republic

[‡]Department of Chemistry, Utrecht University, NL-3584 CH Utrecht, Netherlands

[§]Laboratory of Molecular Transformation, Tohoku University, Aobayama, Aoba-ku, Sendai, Miyagi 980-8578 Japan

Supporting Information



ABSTRACT: A mechanistic pathway for cleavage of the N-glycosidic bond of 8-oxo-2'-deoxyguanosine (oxoG) catalyzed with the human 8-oxoguanine glycosylase 1 DNA repair protein (hOGG1) is proposed in this theoretical study. The reaction scheme suggests direct proton addition to the glycosidic nitrogen N9 of oxoG from the Ne -ammonium of Lys249 residue of hOGG1 that is enabled owing to the N9 pyramidal geometry. The N9-pyramidalization of oxoG is induced within hOGG1 active site. The coordination of N9 nitrogen to the Ne -ammonium of Lys249 unveiled by available crystal structures enables concerted, synchronous substitution of the N9–C1' bond by the N9–H bond. The reaction is compared with other pathways already proposed by means of calculated activation energies. The $\Delta G^\#$ energy for the newly proposed reaction mechanism calculated with the B3LYP/6-31G(d,p) method 17.0 kcal mol⁻¹ is significantly lower than $\Delta G^\#$ energies for other reactions employing attack of the Ne -amino group to the anomeric carbon C1' of oxoG and attack of the Ne -ammonium to the N3 nitrogen of oxoG base. Moreover, activation energy for the oxoG cleavage proceeding via N9-pyramidalization is lower than energy calculated for normal G because the electronic state of the five-membered aromatic ring of oxoG is better suited for the reaction. The modification of aromatic character introduced by oxidation to the nucleobase thus seems to be the factor that is checked by hOGG1 to achieve base-specific cleavage.

INTRODUCTION

The DNA repair is an essential defense mechanism evolved by a cell to preserve integrity of the genetic information in living organisms.¹ One of the major DNA lesions, 8-oxo-2'-deoxyguanosine (oxoG), represents in this respect a serious defect that arises owing to the chemical modification of normal 2'-deoxyguanosine (G) typically caused by various kinds of reactive oxygen species (Figure 1). The damaged nucleobase is known to induce transversion mutation to DNA found in human cancer.² The oxoG lesions in living organisms are repaired with base excision repair (BER) enzymes of oxoG DNA glycosylase/lyase family. The human homologue, called human oxoG glycosylase 1 (hOGG1), targets the oxoG lesions in chromosomal DNA.^{3–10}

The organochemical mechanism of the glycosylase/lyase family in which also belongs the hOGG1 protein was originally

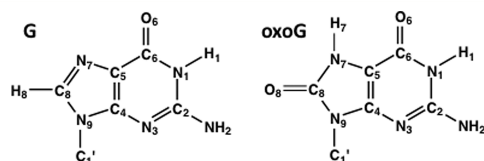


Figure 1. Schematic representation of the chemical structure of 8-oxo-2'-deoxyguanosine (oxoG) and 2'-deoxyguanosine (G).

proposed by Wallace's group.¹¹ The basic idea was later confirmed by Lloyd's group due to detection of the key DNA–enzyme conjugate.¹² This mechanism, adopted for the hOGG1 by Verdine's group, basically proceeds in the following

Received: September 13, 2012

Published: September 18, 2012

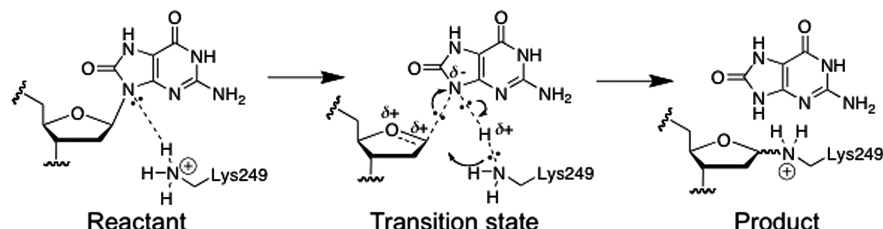
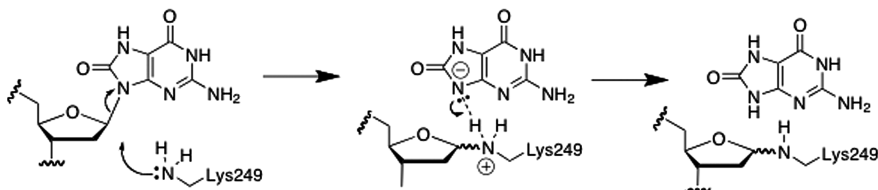
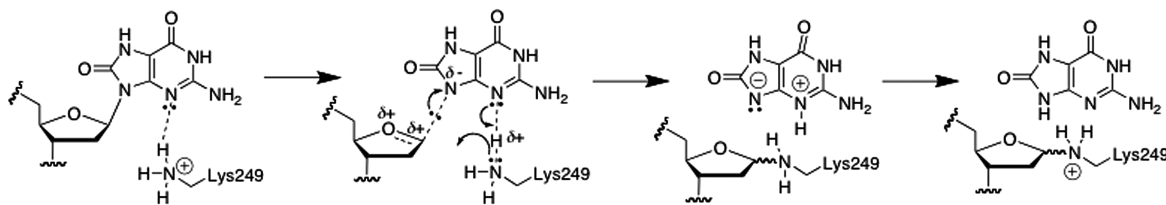
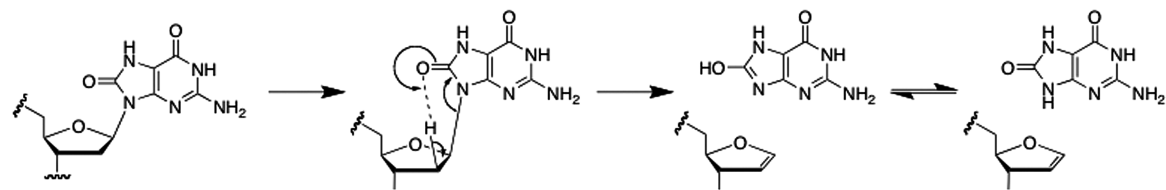
a) σ -bond substitution mechanism**b) C1'-attacked mechanism****c) N3-protonation mechanism****d) Simple dissociation**

Figure 2. Chemical diagrams of the mechanisms for cleavage of N-glycosidic bond of oxoG with hOGG1 calculated in this work. The names introduced here are used throughout the text. (a) σ -Bond substitution mechanism suggested in this work. (b) C1'-attacked mechanism.^{11,12,3,5,18} (c) N3-protonation mechanism.²⁰ (d) Simple dissociation mechanism added only for the sake of comparison with the other Lys249-assisted mechanisms.

order.^{13,14,3} (1) Elimination of a damaged base and formation of a DNA–enzyme conjugate via nucleophilic attack of the ϵ -amino nitrogen of Lys249 (hOGG1) to the anomeric carbon of oxoG. (2) Formation of a Schiff base (a sugar adduct). (3) Cleavage of the defective DNA strand via degradation of the sugar adduct that is followed by DNA dissociation from hOGG1. Among these steps, the first one is irreversible and represents the driving force of the repair mechanism.¹⁴ The mechanism of the base excision is therefore key for resolving whole DNA repair.

Nevertheless, it is currently unclear whether the first glycosylase activity is S_N1- or S_N2-type of reaction because of slow product dissociation from hOGG1.^{14,5} Moreover, the chemical role of Asp268, phylogenetically well-conserved residue among all BER enzymes, is still obscure. Neither the crystal structures of hOGG1¹⁵ nor the structures of its complexes with oxoG-containing DNA^{16–19} unveiled the chemical mechanism of base elimination.

Consequently, different cleavage pathways have been proposed following the insight provided by fundamental crystallographic and biochemical studies. The first mechanism was the classically proposed one, often seen in reaction schemes

linked to the BER enzymes, in which Ne -amino nitrogen of Lys249 (hOGG1) attacks the C1' anomeric carbon (oxoG) to initiate the glycosylase activity (Figure 2b).^{11,12,3,5,18} Another mechanism proposed by Garavelli's group suggests specific stabilization of the leaving nucleobase (Figure 2c).²⁰ The proton addition to N3 (oxoG) suggested by Garavelli is in line with the Verdine's assumption: "Any interaction that would stabilize the incipient negative charge on the oxoG during rupture of the glycosidic bond would facilitate base excision by a dissociative mechanism."¹⁷ On the basis of this generally accepted assumption, various cleavage mechanisms including nonenzymatic hydrolysis of oxoG were modeled theoretically.^{21–26}

The stabilization of substrate in a desired precleavage state is typical for all BER enzymes.¹⁴ The mechanism proposed in this work suggests one particular kind of stabilization employing Ne -ammonium (Lys249), where one of the protons directly attacks the glycosidic nitrogen N9 (oxoG), inducing its pyramidal geometry. Pyramidalization of the glycosidic nitrogen is an existing phenomenon found in the DNA and RNA crystal structures with ultrahigh resolution.²⁷ Structurally, it is enforced by molecular surroundings, as was recently evidenced for

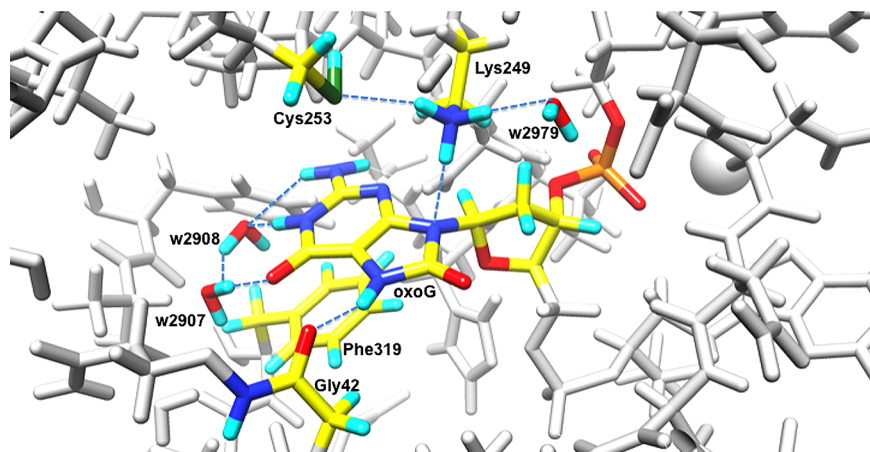


Figure 3. Closeup of oxoG surrounded by hOGG1 residues and water molecules as delivered by the crystal structure with PDB ID 2NOZ.¹⁹ Important interactions were chalked out in blue. Picture shows the structure calculated with QM/QM method.

residues of the DNA G-quadruplex.²⁸ Chemically, it gives rise to concentration of the lone-pair electron density at glycosidic nitrogen and shifts its electronic state from sp^2 -like to sp^3 -like. However, the rehybridization may also provide a basis for direct protonation of the glycosidic nitrogen. The N9 (oxoG) can be thus directly protonated with Ne-ammonium (Lys249), providing its pyramidal geometry during base excision.

Although the mechanisms proposed previously predicted properly experimentally characterized products of the reaction, none of them reflected N9-pyramidalization of oxoG inserted into the hOGG1 catalytic site and all consequences of thereof for base excision. It came out very recently that hOGG1 discriminates between oxoG and normal G with extreme efficiency and that the checkpoint activity could not be explained with the mechanisms already proposed.²⁹ This study aims to provide sound arguments for new chemical mechanism that is energy-efficient and ensures base-specific cleavage of oxoG against normal G with hOGG1.

COMPUTATIONAL METHODOLOGY

Structural Model. The N9-pyramidalization of oxoG inserted into the hOGG1 active site was calculated by using the crystal geometry with PDB ID 2NOZ.¹⁹ The structural model used in QM/QM geometry optimization (see below) included all hOGG1 residues within the 10 Å sphere centered at the glycosidic nitrogen of oxoG. The Lys249, Asp268, Cys253, and Phe319 residues (hOGG1), oxoG, and the water molecules W2979, W2908, and W2907 were included into “inner” QM region during the geometry optimization (Figure 3). These residues were optimized freely, whereas the rest of the hOGG1 residues, describing the “outer” QM region, were fixed in their crystal geometries, ensuring correct explicit surrounding of the inner region. The Lys249 (charge +1) and Asp268 (charge -1) yielded total charge -3 owing to the three phosphate groups, three aspartic acids, and one Ca^{2+} cation in the complex. The inner part included 102 atoms, and the outer part included 650 atoms. The QM/QM optimal geometry can be found in the Supporting Information.

The calculations of different mechanistic pathways were done by employing the crystal structure with PDB ID 1N3C.¹⁷ The structural model included oxoG and Lys249 residues. To ensure the same arrangement of reactants as in the crystal structure, we kept fixed the C3' and C4' carbon atoms (DNA backbone) and the N1, $C\alpha$, and $C=O$ atoms (protein

backbone) in their X-ray geometries during the calculations. Lys249 with the charge +1 (Ne-ammonium) yielded total charge of +1. The pathways employing Ne-amine were complex neutral. The reactant for pathway where Ne-ammonium (Lys249) attacks the N9 nitrogen (oxoG) was calculated using the crystal geometry without any modification. The same initial geometry was also used for the pathway employing Ne-amine (Lys249) attacking C1' (oxoG). The reactant for the pathway employing Ne-ammonium (Lys249) attacking N3 (oxoG) was calculated with slightly modified initial geometry of Lys249, where Ne-ammonium appeared closer to N3 nitrogen (oxoG). The optimal geometry calculated was in this case compatible with the catalytic pocket, as also reported in the original work.²⁰ Important geometry parameters, atomic charges, and bond orders calculated for reactant, transition state, and product along the reaction pathways can be found in the Supporting Information.

QM Calculations. The Morokuma's QM/QM ONIOM approach,³⁰ as implemented in the Gaussian 09 program,³¹ was used in the geometry optimization of oxoG inserted into the hOGG1 catalytic site. The inner QM region was described with the CAM-B3LYP method,³² whereas the outer region was described with the PM6 method. The basis set was 6-31G(d,p).³³ For the sake of comparison of CAM-B3LYP performance with other DFT functionals, the WB97XD³⁴ or M06-2X³⁵ functional was alternatively used for the description of inner part. The geometry optimization proceeded in two steps. The preliminary geometry optimization of only hydrogen atoms added to the crystal structure with the PM6 method was followed by the QM/QM geometry optimization.

The geometries and energies along the reaction pathways were calculated with the B3LYP³⁶ and alternatively with the BPW91³⁷ DFT functional. For the sake of comparison of the method performance in dependence on the atomic basis, we used the 6-31G(d,p), 6-31++G(d,p), and 6-311++G(d,p) basis sets.³³ The implicit solvent-phase model CPCM^{38,39} with a dielectric constant for diethylether was used because it performed successfully in similar studies on modeling overall environmental effects in enzymes.⁴⁰ The transition-state geometries were calculated with the synchronous transit-guided quasi-Newton (STQN) method requiring the initial structures of the reactant and product as an inputs. The validity of all stationary points for reactant, transition state, and product was confirmed with the vibration-frequency calculations. Through-

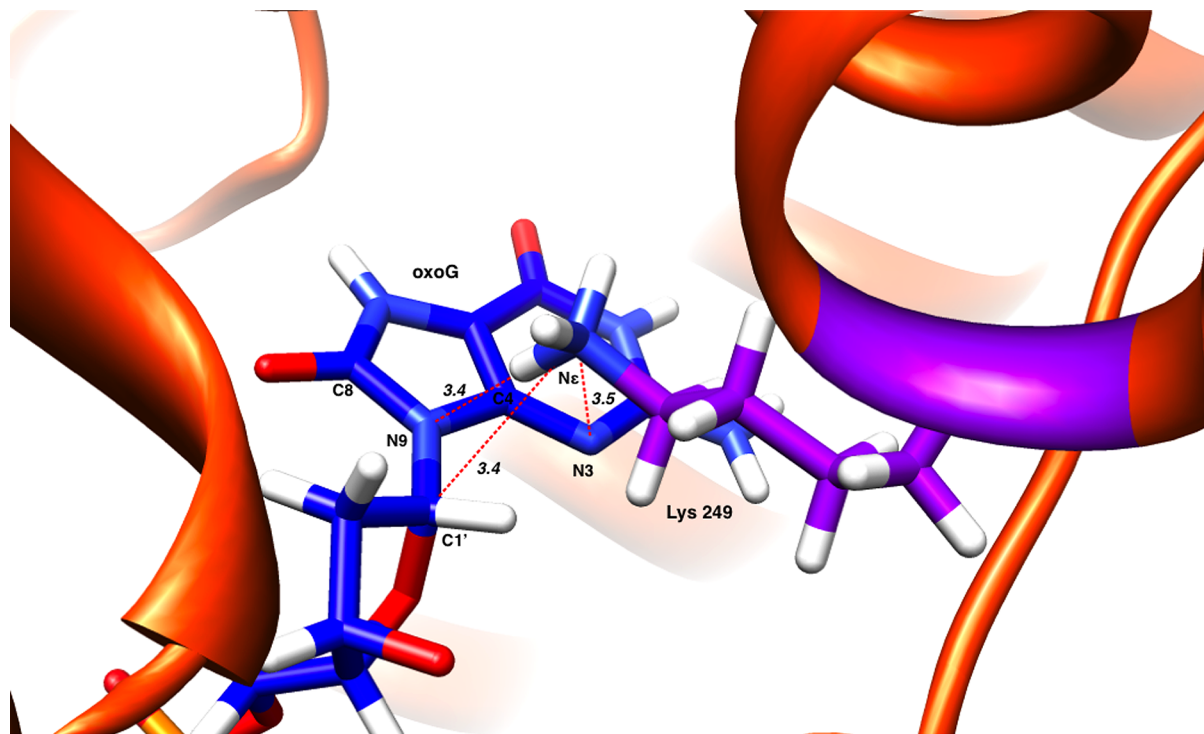


Figure 4. Closeup of oxoG captured in hOGG1 catalytic core as delivered by the crystal structure with PDB ID 1N3C.¹⁷ The distances of Ne nitrogen (Lys249) from the catalytically important atoms of oxoG are in angstroms.

out the text, “non-interacting product” means the enzyme–product dissociated state where the respective calculation was done for separated (isolated) products, whereas “interacting product” means the state in which products still interact, calculated just after the reaction step.

The Gibbs free energy $\Delta G = \Delta H - T\Delta S$ was calculated for room temperature (298.15 K) and pressure 1 atm, where ΔH employed the thermal correction to enthalpy and ΔS was calculated within the ideal-gas, rigid-rotor, and harmonic-oscillator approximation. The activation energy $\Delta G^\#$ was calculated as the difference of the Gibbs free energy for transition state and reactant. The reaction energy ΔG_R was calculated as the difference of the Gibbs free energy for product and reactant. The $\Delta E^\#$ and ΔE_R electronic energies reported in the Supporting Information were calculated correspondingly.

The CAM-B3LYP/PM6 QM/QM geometry optimization and the B3LYP/6-31G(d,p)/CPCM calculations of the reaction pathways were reported in the body text if not specified otherwise. The data obtained with other methods can be found in the Supporting Information. The NBO atomic charges and bond orders characterized with the Wiberg bond indexes⁴¹ were calculated with the natural bond orbital (NBO) analysis⁴² using the NBO program 3.1.⁴³

RESULTS

The base-excision with hOGG1 proceeds through the transition state that is characteristic of all BER enzymes. Upon the N-glycosidic bond cleavage, sugar adopts the cationic, oxocarbenium-like form, whereas nucleobase adopts the anionic form. There is experimental evidence of charge-stabilization provided by BER enzymes that lowers activation barrier of the cleavage.¹⁴ Because the charge-stabilization ensured by the mechanism suggested in this work depends essentially on N9-pyramidalization, we first explore the N9-pyramidalization of oxoG substrate

inserted into the hOGG1 catalytic pocket. Then, we describe the mechanistic pathway in detail and compare it with other competitive pathways considered for the catalytic cleavage previously. Lastly, we compare the N-glycosidic bond cleavage with the newly suggested mechanism for oxoG and normal G.

Residues of hOGG1 Catalytic Pocket Enforce N9-Pyramidalization of OxoG.

The geometry of oxoG trapped in hOGG1 catalytic pocket was described with the X-ray crystallography.^{17,19} The hOGG1 residues of catalytic site include in particular Lys249, Asp268, Cys253, and Phe319 (Figure 3). The hOGG1 residues surrounding oxoG substrate were treated within the inner region in QM/QM geometry optimization. (For details, see the Computational Methodology.) The extent of N9-pyramidalization was evaluated with improper torsion angle κ , defined as $\text{C}4-\text{N}9-\text{C}1'-\text{C}8-180^\circ$ (Figure 1). It follows that idealized, planar configuration of N9 nitrogen corresponds to $\kappa = 0^\circ$, and the extent of N9-pyramidalization is reflected by the increase in absolute value of κ torsion. The opposite signs of κ torsion angle obviously indicate the two antipodal pyramidalizations of N9.

Pyramidalization of the glycosidic nitrogen is a subtle structural effect that can be reliably measured only in crystal structures with the ultrahigh resolution.²⁷ For example, the RNA and DNA structures analyzed in our previous study had resolution 1.0 Å or better and R value better than 0.2. The ultrahigh criteria basically ensured exclusion of all structures refined with the methods employing empirical force-fields because these may show false, typically underestimated pyramidalization.²⁷ Unfortunately, the resolution of 1N3C and 2NOZ structure showing oxoG inserted into the hOGG1 catalytic site was only 2.70 and 2.43 Å, respectively. We can therefore hypothesize that these structures need not show actual N9-pyramidalization of oxoG, albeit they clearly and

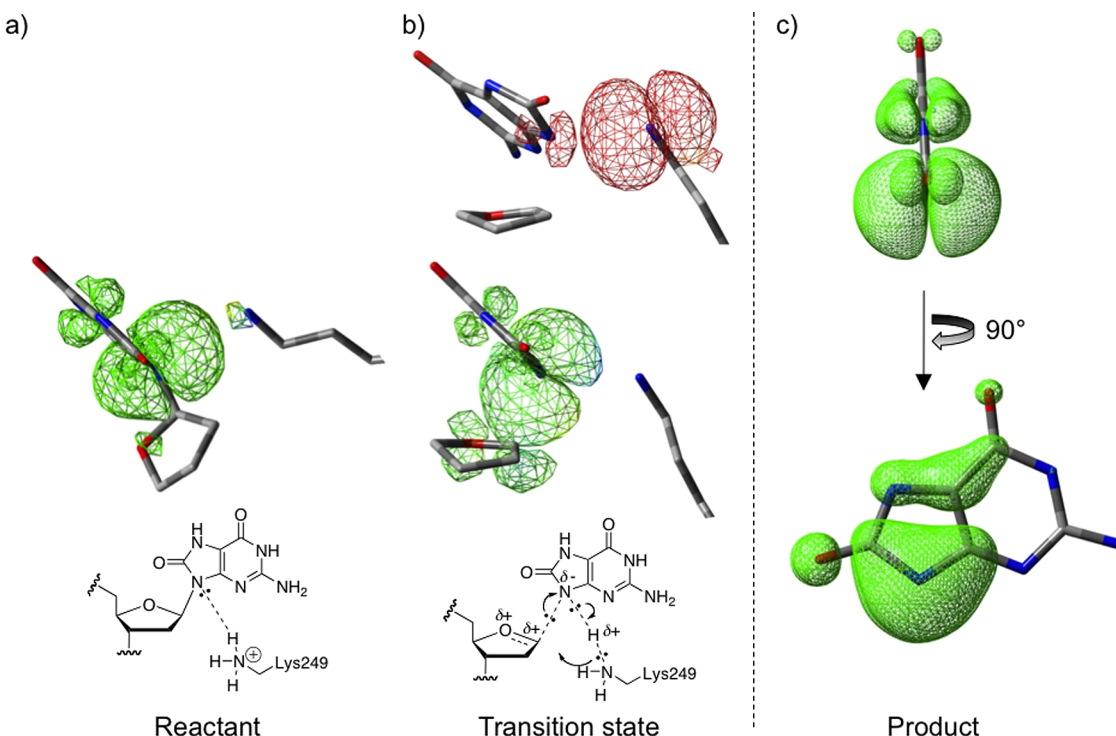


Figure 5. Contour plots of the lone-pair electron orbitals at glycosidic nitrogen N9 of oxoG (green) and Ne nitrogen of Lys249 (red) calculated for (a) reactant, (b) transition state, and (c) product of the σ -bond substitution mechanism suggested in this work. (a) Lone-pair electrons of N9 nitrogen are polarized with the Ne -ammonium group, and the initial interaction $\text{N}9 \cdots \text{H}^+ - \text{N}3$ is established. (b) Glycosidic bond ruptured and the proton formerly associated at Ne -ammonium transferred to N9 nitrogen of oxoG base. The electron lone-pair density of N9 nitrogen is now polarized by the oxocarbenium of deoxyribose. The lone-pair electron orbital of Ne -amine is directed toward oxocarbenium. (c) Lone-pair electron orbital of N9 in oxoG base is symmetric with respect to the base plane.

reliably define all substrate–enzyme interactions within the catalytic core (Figure 3).

The N9-pyramidalization measured in the crystal structures was small; the κ torsion in 1N3C and 2NOZ structures was 1.9 and 2.8° , respectively. The N9-pyramidalization calculated with the QM/QM method (CAM-B3LYP/PM6) yielded the optimal value of κ torsion of 38.8° . We think that the calculated N9-pyramidalization is reliable because the complete surroundings of oxoG are known, and QM calculations provide in such case accurate values of κ torsion. The calculations in our recent study reproduced even stereoinversion of N9 for G residues of DNA G-quadruplex, where magnitudes of N9-pyramidalization were much smaller. (For details, see ref 28 and the Discussion below.)

The configuration of N9 for oxoG doped into hOGG1 was such that pyramid with the N9 on top was directed toward the H– Ne bond (Lys249) so that these three atoms were aligned almost linearly (Figures 3 and 4). The calculated N9–H– Ne angle was 168° , and the $r_{\text{N}9-\text{H}(\text{Ne})}$ distance was 2.00 \AA . This initial coordination of N9 (oxoG) to Ne -ammonium (Lys249) appeared to be essential for the cleavage mechanism (see later). Other geometry parameters describing oxoG trapped in the hOGG1 catalytic pocket changed only a little during the geometry optimization (Supporting Information). Importantly, the $r_{\text{Ne}-\text{N}9}$, $r_{\text{Ne}-\text{N}3}$, and $r_{\text{Ne}-\text{C}1'}$ distances changed less than 0.08 \AA (Figure 4). The geometry optimization thus provided plausible arguments for actual pyramidal arrangement of N9 (oxoG), keeping the original substrate-hOGG1 geometry practically the same as that in the crystal structure.

Mechanistic Pathway Employing N9-Pyramidalization of OxoG. The Lys249 is the key catalytic residue of hOGG1.

When it was mutated, the repair ability was lost.¹⁴ The crystal geometries unveiled possible attack of Lys249 to all three catalytically important sites (Figure 4). The three different cleavage mechanisms can be thus initiated; the N9 or N3 nitrogen can be attacked with Ne -ammonium, and the C1' carbon can be attacked with Ne -amine. To obtain a complex picture of the Lys249 catalytic role, the three pathways were calculated. These calculations allowed consistent comparison of the respective activation energies (Figure 6). The mechanism where Lys249 attacks directly the N9 nitrogen of oxoG was referred to here as the σ -bond substitution mechanism. The mechanism where C1' carbon is attacked with the Ne -amine, suggested for hOGG1 by Verdine¹⁸ in accord with the Lloyd's reaction scheme,¹² was referred to as the C1'-attacked mechanism. The mechanism employing the preactivation step where N3 nitrogen is protonated with Ne -ammonium, suggested by Garavelli,²⁰ was referred to as the N3-protonation mechanism. The N-glycosidic bond cleavage without stabilization provided by Lys249, included here only for the sake of comparison with other pathways is referred to as simple dissociation. The respective reaction schemes are shown in Figure 2. Another mechanism assuming proton-addition to the O8 oxygen of oxoG was not included here because the respective calculated activation energy was fairly large.^{44,45}

The σ -bond substitution pathway was initiated with direct coordination of Ne -ammonium (Lys249) to N9 (oxoG). The Ne -ammonium coordinated spontaneously to N9 in the geometry optimization employing the crystal geometry. The mode of initial interaction calculated for oxoG and Lys249 and that obtained employing all residues of hOGG1 catalytic pocket (QM/QM calculation) was the same. The cation–lone-pair

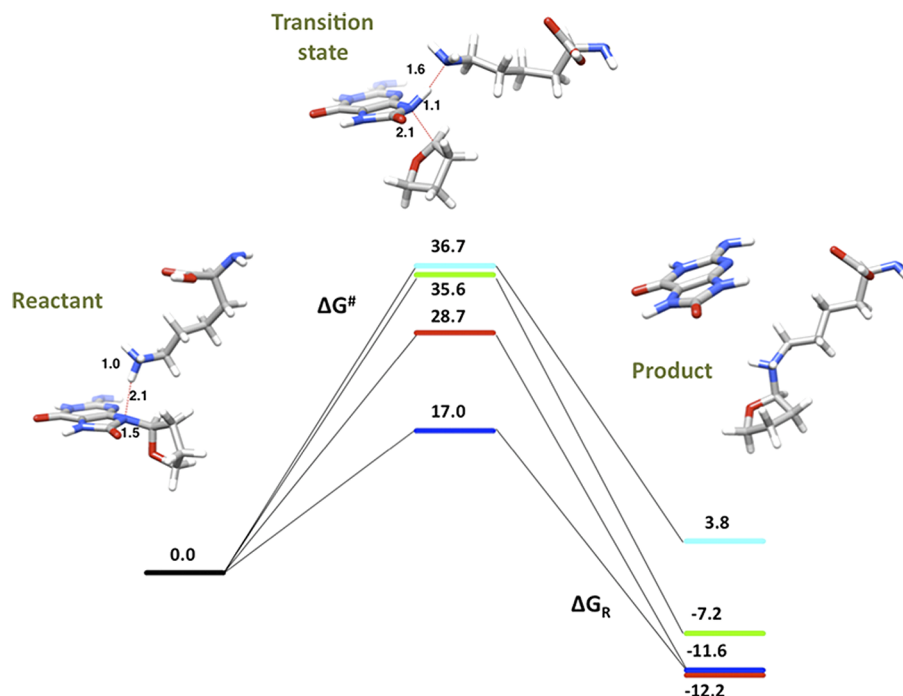


Figure 6. Energy profiles calculated along reaction pathways for N-glycosidic bond cleavage of oxoG: the σ -bond substitution (blue), the C1'-attacked mechanism (green), the N3-protonation mechanism (red), the simple dissociation mechanism (light blue). The Gibbs free energies of the activation and reaction ΔG^\ddagger and ΔG_R are in kcal mol⁻¹. The respective geometries for the σ -bond substitution mechanism are shown with the $r_{\text{C}1'-\text{N}9}$, $r_{\text{N}9-\text{H}}$, and $r_{\text{H}-\text{Ne}}$ distances in angstroms.

electron interaction suggested already by Verdine¹⁷ enforced the pyramidal geometry of N9 (oxoG); $\kappa = 37.1^\circ$, $\text{N}9-\text{H}-\text{Ne} = 165.6^\circ$. Note that the N9-pyramidalization calculated for oxoG only was much smaller and antipodal; $\kappa = -7.2^\circ$ (reactant of simple dissociation, see Supporting Information).

In the transition state where the N9-pyramidalization was maximal, $\kappa = 65.7^\circ$, the proton of Ne-ammonium transferred to N9 (oxoG). To demonstrate the extent of N9-pyramidalization, we also calculated the sum of three adjacent valence angles C1'-N9-C4, C4-N9-C8, and C8-N9-C1'. The zero N9-pyramidalization assuming this sum equals 360° , but for the reactant and transition state it was 351° and 321° , respectively. The idealized sp^3 -like geometry for methane assumes that the sum of respective valence angles is roughly 330° . The transition-state geometry of N9 (oxoG) is therefore truly sp^3 -like.

The $r_{\text{C}1'-\text{N}9}$ bond length calculated for the transition state was 2.09 Å; for the reactant it was 1.47 Å, and the X-ray showed 1.46 Å. The oxoG release was followed by spontaneous capture of Ne-ammonium with oxocarbenium (Figure 5). The activation energy ΔG^\ddagger calculated for the noninteracting products was 17.0 kcal mol⁻¹, and the reaction energy ΔG_R was -11.6 kcal mol⁻¹. The same ΔG^\ddagger energy 17.1 kcal mol⁻¹ was estimated from the original experiment.²⁰ In any case, we have to mention that variation of the ΔG^\ddagger energies calculated with QM methods employing different DFT functionals and basis sets exists. However, the relative order of the ΔG^\ddagger energies for the three reaction mechanisms appeared to be method-independent (Supporting Information). The σ -bond substitution mechanism was therefore consistently linked to the lowest ΔG^\ddagger energy (Figure 6).

The initiation of the C1'-attacked mechanism proceeded via attack of anomeric C1' carbon (oxoG) with Ne-ammonium (Lys249) according to the Verdine's proposal (Lloyd's original

scheme¹²).¹⁸ The initial coordination of Ne-amine to C1' was calculated again spontaneously. The calculated $r_{\text{Ne}-\text{C}1'}$ distance in the reactant was 3.53 Å, longer by 0.16 Å as compared with the crystal geometry. The $r_{\text{N}9-\text{C}1'}$ bond length calculated for the reactant was 1.47 Å, and in the transition state it was 2.42 Å. The calculated ΔG^\ddagger energy was 35.6 kcal mol⁻¹. The hydrogen of Ne-amine pointing toward the N9 nitrogen of oxoG migrated to this atom during the optimization of products. The same intermediate has been previously reported.¹⁸ The ΔG_R -5.4 kcal mol⁻¹ was calculated for the interacting products, $r_{\text{N}9-\text{C}1'} = 3.63$ Å and $r_{\text{C}1'-\text{N}3} = 1.48$ Å, whereas for separated, noninteracting products it was -7.2 kcal mol⁻¹.

The reactants of the N3-protonation mechanism were calculated assuming the proposal by Garavelli.²⁰ The starting geometry was prepared via modification of the crystal geometry; the Lys249 was a little more directed toward N3 (oxoG), and the proton of Ne-ammonium was transferred to N3 (oxoG). Then, the geometry optimization proceeded successfully, yielding reliable geometry of the reactants: $r_{\text{Ne}-\text{N}3} = 2.79$ Å, $r_{\text{Ne}-\text{H}(\text{N}3)} = 1.73$ Å, $r_{\text{C}1'-\text{N}3} = 3.82$ Å, and $r_{\text{N}9-\text{C}1'} = 1.47$ Å. In the course of geometry optimization, actually two, slightly different, optimal geometries were calculated. (Note the $r_{\text{Ne}-\text{C}1'}$ distances for the mechanism in the Supporting Information.) Because the respective ΔG^\ddagger and ΔG_R energies were practically the same, we report hereafter only the calculation with slightly lower ΔG^\ddagger . The $r_{\text{N}9-\text{C}1'}$ bond length calculated in the transition state was 2.26 Å, and the $r_{\text{C}1'-\text{N}3}$ distance was 2.68 Å. The calculated ΔG^\ddagger energy was 28.7 kcal mol⁻¹. The ΔG_R for the interacting products was 7.9 kcal mol⁻¹ because the intermediate requires stabilization via the cascade reaction proposed by Garavelli.²⁰ The cascade reaction was not calculated in this study. We calculated only ΔG_R for the final, noninteracting products, -12.2 kcal mol⁻¹.

The simple dissociation mechanism was included only for the sake of comparison with other reactions. It reports only intrinsic cleavability of the N-glycosidic bond in oxoG. The $r_{\text{C}1'-\text{N}9}$ bond length of 1.46 Å calculated for the reactant (the optimal geometry of *anti*-oxoG) was the same as that in the crystal structure. The glycosidic torsion χ was 252°; in the crystal it was 275°. In the transition state, the $r_{\text{C}1'-\text{N}9}$ was 2.69 Å and $\Delta G^\#$ energy was 36.7 kcal mol⁻¹. During the geometry optimization of products (oxcarbenium and oxoG⁻), the proton at C2' sugar carbon transferred to O8 (oxoG), indicating clearly the lack of the charge-compensation for oxoG. The ΔG_R energy 3.8 kcal mol⁻¹ calculated for this oversimplified model was obviously unreliable, as the products could not be stabilized properly. Nevertheless, the $\Delta G^\#$ energy was useful for a comparison with the $\Delta G^\#$ energies for rational, Lys249-assisted pathways.

Cleavage of N-Glycosidic Bond in OxoG and Normal G. The geometry optimization of reactants started with the X-ray geometry 1N3C but employed G instead of oxoG. In this case, the Ne-ammonium coordinated spontaneously to N3 (G). The electronic state of G hampered initiation of the σ -bond substitution reaction. (See the Discussion.) It follows that the proper reactants could not be calculated spontaneously and the computational strategy had to be modified. (1) The calculated dependence of total energy on length of N-glycosidic bond $r_{\text{C}1'-\text{N}9}$ was used for comparison of N-glycosidic bond cleavability in oxoG and G. (2) The initial coordination of Ne-ammonium to N9 (G) needed for σ -bond substitution reaction was achieved only after the increased N9-pyramidalization was enforced with κ torsion constrained during the calculations (Figure 7). (See also the explanatory caption of the Figure.)

According to the grid-point geometry optimization for $r_{\text{C}1'-\text{N}9}$ elongated stepwise, the maximum of cleavage barrier for both G and oxoG occurred at $r_{\text{C}1'-\text{N}9} \approx 2.1 Å. It basically agreed with the geometry for transition state of oxoG employing the σ -bond substitution ($r_{\text{C}1'-\text{N}9} = 2.09 Å). The comparison of cleavage barriers for G and oxoG was therefore done for the calculations where $r_{\text{C}1'-\text{N}9} = 2.1 Å.$$$

The extent of N9-pyramidalization enforced now with constrained κ torsion altered energy barriers for oxoG and G significantly. As compared with the barrier for oxoG with freely evolving N9-pyramidalization (unconstrained κ , open red circle, Figure 7), the barrier increased by 2.5 kcal mol⁻¹ when κ was fixed to 40° (filled red circle, Figure 7), whereas it decreased by 1.6 kcal mol⁻¹ when κ was 60° (red square, Figure 7). The value of κ torsion calculated for the true transition state of oxoG employing the σ -bond substitution was 66°. (Here we mean the calculation of exact transition state confirmed by the frequency calculation in the previous paragraph.) The difference between the barriers for G with κ fixed to 60° (blue square, Figure 7) and 50° (blue triangle, Figure 7) was 3.0 kcal mol⁻¹.

The energy barriers for cleavage of oxoG and G differed significantly. The energy barrier for G calculated with the same constraint was always larger as compared with that for oxoG. For $\kappa = 60^\circ$, it was by 2.3 kcal mol⁻¹, and for $\kappa = 50^\circ$ it was by 4.0 kcal mol⁻¹. The smaller was N9-pyramidalization; the larger was the difference between respective energy barriers for oxoG and G. The π -character of nucleobase influencing N9-pyramidalization is therefore closely related to the intrinsic cleavability of the N-glycosidic bond in oxoG and G.

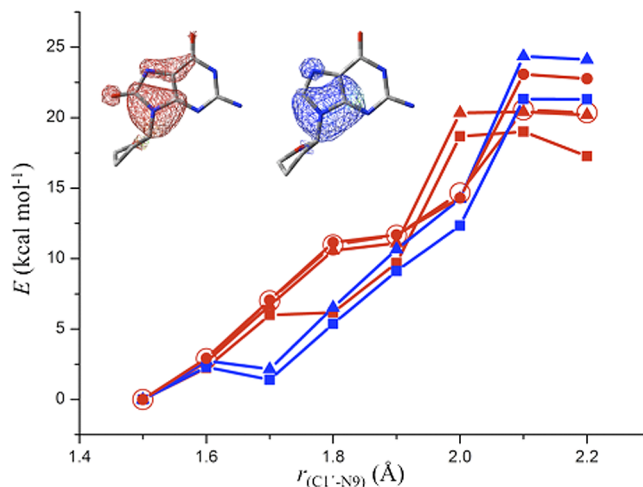


Figure 7. Energy barriers calculated for N-glycosidic bond cleavage of oxoG and G employing σ -bond substitution mechanism and the contour plots of lone-pair electron orbital at N9 for oxoG (red) and G (blue). The dependences of energy on glycosidic bond length $r_{\text{C}1'-\text{N}9}$ calculated for oxoG (red lines) and G (blue lines) are related to the energies for $r_{\text{C}1'-\text{N}9} = 1.5 Å. Local character of the orbital for oxoG is consistent with its more distinctive sp³-like state as compared with that for normal G. (See the Discussion.) The N9-pyramidalization was increased and constrained by fixing the improper torsion angle $\kappa = \text{C}4-\text{N}9-\text{Cl}'-\text{C}8 - 180^\circ$. The κ torsion in oxoG was 60° (red ■), 50° (red ▲), and 40° (red ●), whereas in G it was 60° (blue ■) and 50° (blue ▲). The more distinctive sp³-like state for oxoG allowed spontaneous attack of Lys249 to N9 when κ was 40° and when it was not constrained (red ○). The unconstrained calculation showed gradual increase in N9-pyramidalization with elongation of the glycosidic bond: $(r_{\text{C}1'-\text{N}9}, \kappa) = (1.5$ Å, 37°), (1.6 Å, 43°), (1.8 Å, 48°), (2.0 Å, 61°), and (2.1 Å, 66°). The bumps between $r_{\text{C}1'-\text{N}9} = 1.6$ and 1.9 Å appeared owing to geometry relaxation of Lysine 249; however, the final geometries of Lysine 249 in all grid-point calculations were equivalent.$

DISCUSSION

The DNA-hOGG1 crystal structures unveiled Lys249 faced toward the five-membered ring of oxoG in such a way that the distances of Ne nitrogen from N9, N3, and C1' atoms were all practically the same (Figure 4).^{17,18} This particular arrangement allowed initiation and in silico realization of three competitive mechanisms linked consistently to the experimentally justified coordination of Lys249 (Figure 2).

The catalytic role of the Lys249 is primarily determined by its charge. The Ne-ammonium was originally proposed to interact with the five-membered ring of oxoG via cation- π interaction.¹⁷ Alternatively, the Ne-amine could attack the C1' sugar carbon of oxoG.¹⁸ The Ne-ammonium form should probably be dominant in hOGG1. (We refer the reader to the analysis of NMR data in ref 44, for example.) The mechanisms employing Ne-ammonium for stabilization of substrate in this study should therefore be more probable than that employing Ne-amine.

The nonspecific cation- π interaction of Ne-ammonium with oxoG should be converted in the course of cleavage to some specific interaction that ensures compensation of oxoG negative charge and provides basis for economic protonation of N9 (oxoG) because the final product is neutral.¹⁴ The two mechanisms employing Ne-ammonium in this way were calculated here: the σ -bond substitution and the N3-protonation mechanism. Chemically, the N3-protonation

differed from the C1'-attacked mechanism de facto only by initial protonation of N3 (oxoG). The bond cleavage was operated with attack of Ne-amine to C1' (oxoG) in both cases. Unlike the N3-protonation, the σ -bond substitution proceeded in single-step (Figure 2) with the lowest activation barrier (Figure 6) because effective charge stabilization occurred directly at N9 (oxoG).

The calculated $\Delta G^\#$ energies depended critically on the mode of charge compensation employed for leaving base. The C1'-attacked mechanism with neutral Lys249 had in this sense only limited capability. The respective $\Delta G^\#$ energy appeared therefore close to that for simple dissociation lacking stabilization completely. The N3-protonation ensured charge compensation but relatively far from the N9 nitrogen. Moreover, this manner of charge-stabilization remained rather uniform during cleavage as compared with that provided by σ -bond substitution (see later). The respective $\Delta G^\#$ energy therefore appeared between those for C1'-attacked and σ -bond substitution mechanisms. The σ -bond substitution ensured effective charge compensation at the most critical site that was furthermore smooth during cleavage because the proton of Ne-ammonium instantaneously responded to the developing negative charge at N9 until the C1'-N9 bond ruptured.

The rearrangement of initial sp^2 -like geometry for N9 (oxoG) toward sp^3 -like in the transition state was essential for the substitution of the N9-C1' bond. The N9-pyramidalization was basically promoted with Lys249 ($\kappa = 37.1^\circ$); the same pyramidal geometry was calculated for oxoG doped in hOGG1 catalytic site ($\kappa = 38.8^\circ$). In any case, the calculated N9-pyramidalization was much larger than that in the crystal structures ($\kappa = 1.9^\circ$, $\kappa = 2.8^\circ$). One may therefore argue against the cleavage mechanism because its key structural feature seems to be incompatible with the crystallographic data. As mentioned above, capturing the N9-pyramidalization with X-ray crystallography puts rather extreme requirements on structure quality. The ultrahigh resolution must be requested.²⁷ Fortunately, all interactions of oxoG within the hOGG1 catalytic core were clearly determined in the crystal structures. Once the structural information was available, it was possible to calculate N9-pyramidalization. The accuracy of the QM calculations was exemplified elsewhere. For example, the N9-pyramidalization of G residues in the crystal geometry of DNA G-quadruplex was explained with QM calculations as the effect of specific molecular environment.²⁸ We therefore hypothesize that the residues of the hOGG1 active site enforced sizable N9-pyramidalization of oxoG. Moreover, the existence of notable N9-pyramidalization was evidenced by the oxidized nucleobase experimentally. The crystals of 9-ethyl-8-hydroxyguanine showed accurately the N9-pyramidalizations depending on hydration and crystal packing; $\kappa = 1^\circ$ in CSD ID FURGAA01, $\kappa = 3^\circ$ in CSD ID FURGAA02, and $\kappa = 29^\circ$ in CSD ID JICLAI.⁴⁶

The basic idea of σ -bond substitution mechanism seems to contradict the common intuition of a chemist anyway. The suggested N9 protonation of oxoG may be regarded unacceptable because other sites like O8, O6, or N3 would be protonated preferentially.⁴⁷ The microscopic pKa values in enzymes may differ from those in bulk, which explains the capability of enzymes to protonate substrate site-specifically.¹⁴ In this respect, the coordination of Lys249 and stabilization role of other residues within hOGG1 catalytic core appeared to be essential. The Gly42 and Phe319 along with the water molecules w2907 and w2908 in the Watson-Crick edge of oxoG hinder the rotation of the nucleobase over the glycosidic

bond (Figure 3). At the same time, these residues probably prevent pyramidal inversion of N9 that would be unfavorable for the reaction. (We may hypothesize that pyramidal inversion of N9 in hOGG1 is controlled in a similar way, as was reported for the trivalent nitrogen in aziridines.⁴⁸) The N9-pyramidalization was induced particularly with Lys249, whose geometry was constrained with the Cys253 and structural water w2979 (Figure 3). The suggested reaction therefore represents a typical enzymatic reaction that could be hardly possible without tight structural constraints provided by hOGG1 catalytic core. This issue became critical for G as a substrate of hOGG1 (see later).

The increase in N9-pyramidalization during cleavage was accompanied by change of the electronic structure of oxoG. The zero N9-pyramidalization calculated for reaction product was reflected by an ideally symmetric lone-pair electron orbital at N9 (Figure 5). Nearly symmetrical orbital was also calculated for oxoG being reactant of the simple dissociation mechanism (not shown.) The increase in inherently small N9-pyramidalization enforced to the reactant with Lys249 was accompanied by loss of the orbital symmetry because lone-pair electrons of N9 experienced proton of Ne-ammonium (Figure 5). The electronic state of N9 shifted toward sp^3 -like, and the N9-C4 and N9-C8 bond orders decreased (Supporting Information). This trend continued in the transition state, where proton of Ne-ammonium transferred to N9 (oxoG) and the bond order of newly formed N9-H bond exceeded that of C1'-N9. The lone-pair electron orbital of formally neutral oxoG base was polarized again, now by the oxocarbenium (Figure 5). The C1'-N9 and N9-H stretching vibrations joined in one antisymmetric vibration, indicating clearly the reaction coordinate. (The movie is available from authors on request.) In other words, elongation of the C1'-N9 bond was immediately followed by proton transfer from Ne-ammonium toward N9, and shortening of the C1'-N9 bond was followed by proton departure from N9 in a synchronous manner. The behavior of the reaction coordinate is compatible with single-step substitution of N-glycosidic bond. Because the lone-pair electron orbital of Ne nitrogen was conveniently faced toward oxocarbenium (Figure 5), the Ne-amine was readily captured by oxocarbenium, leaving oxoG nucleobase free for dissociation. The charge stabilization during reaction was smooth because it proceeded on demand of departing oxoG base. The optimal cleavage conditions were also reflected by the shortest $r_{C1'-N9}$ distance of 2.09 Å in the transition state as compared with that for N3-protonation (2.26 Å and 2.68 Å), C1'-attacked (2.42 Å), and simple dissociation mechanism (2.69 Å).

Rearrangement of the lone-pair electrons at N9 (oxoG) during reaction obviously depends on overall distribution of all electrons within the aromatic ring. One can thus foresee that different aromatic character of nucleobase should affect the cleavage. Actually, it turned out that Lys249 probed the electronic states of oxoG and G selectively. (1) The electronic state of G hampered the reaction in contrast with that of oxoG, which promoted initiation spontaneously. Explanation: the N9 lone-pair electrons of G are more delocalized within the five-membered ring, and their polarization with Ne-ammonium is therefore difficult (Figure 7). (2) The extent of N9-pyramidalization affected cleavage barriers for oxoG and G in the same way. The larger was N9-pyramidalization; the smaller was reaction barrier. Explanation: the N9-pyramidalization and hybridization state of the lone-pair electrons at N9 are closely related. The enforced increase in N9-pyramidalization shifts

electronic state of the lone-pair electrons toward sp^3 , which enhances the bond cleavage. (3) The N9–C1' bond orders calculated in oxoG and G were similar, but the N9–C8 and N9–C4 orders of inner-ring bonds were smaller in oxoG. Implication: although the N-glycosidic bonds in oxoG and G are virtually very similar, the bonding within the five-membered aromatic ring actually enhances (oxoG) or hinders (G) the substitution of N9–C1' by N9–H bond. (4) The cleavage barrier for G was consistently higher than that for oxoG.

The increase in N9-pyramidalization enforced here in a very simple way with constrained κ torsion angle resulted in the decrease in energy barrier for the cleavage. The glycosidic nitrogen of G has distinctive sp^2 -like character with delocalized lone-pair electrons, which can be hardly attacked with $N\epsilon$ -ammonium. The oxidative damage of G therefore seems to open a rather specific way for its repair with all attributes reported here for oxoG cleavage. However, besides the intrinsic aromatic character of a nucleobase, the external enforcement of N9-pyramidalization might further decrease cleavage barrier. The interaction of Gly42 carbonyl with N7–H of oxoG (Figure 3) known to be essential for the lesion recognition¹⁴ or some other suitable interaction might possibly enforce additional N9-pyramidalization during the cleavage. At the moment we can only hypothesize whether the N9-pyramidalization could be controlled in this way by hOGG1 residues interacting with substrate, but if so, the cleavage barrier would be further scaled down.

In the calculations for cleavage of G, we employed the DNA-hOGG1 crystal geometries for oxoG, where the deposition of substrate was convenient for cleavage reaction. However, the hOGG1 does not favor G as substrate. The crystal structures available for G inserted into hOGG1, the PDB ID 1YQK⁵⁰ and 3IH7,²⁹ showed significantly alternated catalytic core (Supporting Information). In the 1YQK structure, the distance of $N\epsilon$ (Lys249) from N9, N3, and C1' was 5.18, 5.53, and 4.19 Å, respectively. The Lys249 interacting here with G24 phosphate and lacking stabilization by Cys253 ($r_{N\epsilon-S(Cys253)} = 5.12$ Å) showed likely initiation of C1'-attacked mechanism. The 3IH7 structure showed a less deformed catalytic site where the distance of $N\epsilon$ from N9, N3 and C1' was 4.18, 3.51, and 4.29 Å, respectively. The $N\epsilon$ nitrogen coordinated here to N3 showed likely initiation of N3-attacked mechanism. The $r_{N\epsilon-N3}$ for G in 3IH7 was 3.51 Å, and the $r_{N\epsilon-N3}$ for oxoG in 1N3C was 3.47 Å. The incompatibility of normal G occurred most probably owing to repulsion between N7 (G) and carbonyl of Gly42 that can be foreseen even from the deposition of oxoG in hOGG1 (Figure 3). Verdine and workers recently reported the existence of an unknown checkpoint mechanism preventing excision of normal G forcibly inserted into hOGG1 active site.²⁹ Despite the fact that G was detected within the catalytic core, the bond cleavage did not occur. The sustainability of N-glycosidic bond reported for G substrate cannot be explained with the C1'–N9 bond orders calculated for G and oxoG in this study (Supporting Information). Actually, even the opposite trend was actually measured. The bond of G was found to be more labile toward hydrolysis as compared with that of oxoG.⁴⁹ These facts strongly suggest some other pathway that is chemically different from N3-attacked and C1'-attacked mechanisms. The pathway proposed in this work may explain the observed checkpoint mechanism: (1) owing to the requirement of precise substrate embedding that is impossible for G and (2) owing to the checked aromatic character of inserted nucleobase that is critical for G.

CONCLUSIONS

The mechanistic pathway proposed in this work suggests that excision of oxoG nucleobase operated with hOGG1 BER enzyme proceeds via state with notably pyramidal geometry of the glycosidic nitrogen. The role of N9-pyramidalization during the glycosidic bond cleavage is essential. The N9-pyramidalization is enforced within the hOGG1 catalytic core, which allows single-step substitution of the N-glycosidic bond with N9–H bond. The reaction was linked with lowest activation energy as compared with other competitive pathways. It was proposed that aromatic character of the nucleobase inserted into the hOGG1 catalytic site is checked to achieve the base-specific cleavage of oxoG against normal G.

ASSOCIATED CONTENT

Supporting Information

Selected geometry parameters, calculated atomic charges and bond orders, comparison of the σ -bond substitution geometries with the crystal geometries, and complete ref 31. This material is available free of charge via the Internet at <http://pubs.acs.org>.

AUTHOR INFORMATION

Corresponding Author

*Phone: 00420 220183234. E-mail: vladimir.sychrovsky@uochb.cas.cz.

Notes

The authors declare no competing financial interest.

ACKNOWLEDGMENTS

This work was supported by the Grant Agency of the Czech Republic P205/10/0228 and by Academy of Sciences of the Czech Republic M200551205. Y.T. and V.S. acknowledge the Young Investigator's Grant of the Human Frontier Science Program (HFSP).

REFERENCES

- (1) Lindahl, T.; Wood, R. D. *Science* **1999**, 286, 1897.
- (2) Hainaut, P.; Hernandez, T.; Robinson, A.; Rodriguez-Tome, P.; Flores, T.; Hollstein, M.; Harris, C. C.; Montesano, R. *Nucleic Acids Res.* **1998**, 26, 205.
- (3) Nash, H. M.; Bruner, S. D.; Scharer, O. D.; Kawate, T.; Addona, T. A.; Sponner, E.; Lane, W. S.; Verdine, G. L. *Curr. Biol.* **1996**, 6, 968.
- (4) Bjoras, M.; Luna, L.; Johnson, B.; Hoff, E.; Haug, T.; Rognes, T.; Seeberg, E. *EMBO J.* **1997**, 16, 6314.
- (5) Nash, H. M.; Lu, R. Z.; Lane, W. S.; Verdine, G. L. *Chem. Biol.* **1997**, 4, 693.
- (6) Lu, R. Z.; Nash, H. M.; Verdine, G. L. *Curr. Biol.* **1997**, 7, 397.
- (7) Boiteux, S.; Radicella, J. P. *Arch. Biochem. Biophys.* **2000**, 377, 1.
- (8) Leipold, M. D.; Muller, J. G.; Burrows, C. J.; David, S. S. *Biochemistry* **2000**, 39, 14984.
- (9) Shinmura, K.; Yokota, J. *Antioxid. Redox Signaling* **2001**, 3, 597.
- (10) Menoni, H.; Shukla, M. S.; Gerson, V.; Dimitrov, S.; Angelov, D. *Nucleic Acids Res.* **2012**, 40, 692.
- (11) Kow, Y. W.; Wallace, S. S. *Biochemistry* **1987**, 26, 8200.
- (12) Dodson, M. L.; Michaels, M. L.; Lloyd, R. S. *J. Biol. Chem.* **1994**, 269, 32709.
- (13) Stivers, J. T.; Jiang, Y. L. *Chem. Rev.* **2003**, 103, 2729.
- (14) Berti, P. J.; McCann, J. A. B. *Chem. Rev.* **2006**, 106, 506.
- (15) Bjoras, M.; Seeberg, E.; Luna, L.; Pearl, L. H.; Barrett, T. E. J. *Mol. Biol.* **2002**, 317, 171.
- (16) Bruner, S. D.; Norman, D. P. G.; Verdine, G. L. *Nature* **2000**, 403, 859.
- (17) Norman, D. P. G.; Chung, S. J.; Verdine, G. L. *Biochemistry* **2003**, 42, 1564.

- (18) Fromme, J. C.; Bruner, S. D.; Yang, W.; Karplus, M.; Verdine, G. *L. Nat. Struct. Biol.* **2003**, *10*, 204.
- (19) Radom, C. T.; Banerjee, A.; Verdine, G. L. *J. Biol. Chem.* **2007**, *282*, 9182.
- (20) Calvaresi, M.; Bottani, A.; Garavelli, M. *J. Phys. Chem. B* **2007**, *111*, 6557.
- (21) Schyman, P.; Danielsson, J.; Pinak, M.; Laaksonen, A. *J. Phys. Chem. A* **2005**, *109*, 1713.
- (22) McCann, J. A. B.; Berti, P. J. *J. Am. Chem. Soc.* **2008**, *130*, 5789.
- (23) Chen, Z. Q.; Zhang, C. H.; Xue, Y. *J. Phys. Chem. B* **2009**, *113*, 10409.
- (24) Millen, A. L.; Wetmore, S. D. *Can. J. Chem.* **2009**, *87*, 850.
- (25) Shim, E. J.; Przybylski, J. L.; Wetmore, S. D. *J. Phys. Chem. B* **2010**, *114*, 2319.
- (26) Rios-Font, R.; Bertran, J.; Sodupe, M.; Rodriguez-Santiago, L. *Theor. Chem. Acc.* **2011**, *128*, 619.
- (27) Sychrovsky, V.; Foldynova-Trantirkova, S.; Spackova, N.; Robeyns, K.; Van Meervelt, L.; Blankenfeldt, W.; Vokacova, Z.; Sporer, J.; Trantirek, L. *Nucleic Acids Res.* **2009**, *37*, 7321.
- (28) Sychrovsky, V.; Vokacova, Z. S.; Trantirek, L. *J. Phys. Chem. A* **2012**, *116*, 4144.
- (29) Crenshaw, C. M.; Kwangho, N.; Kimberly, O.; Kutchikian, P. S.; Bowman, B.; Karplus, M. *J. Biol. Chem.* **2012**, *287*, 24916.
- (30) Vreven, T.; Byun, K. S.; Komaromi, I.; Dapprich, S.; Montgomery, J. A.; Morokuma, K.; Frisch, M. J. *J. Chem. Theory Comput.* **2006**, *2*, 815.
- (31) Frisch, M. J.; et al. *Gaussian 09*, revision B.01; Gaussian Inc.: Wallingford, CT, 2009.
- (32) Yanai, T.; Tew, D. P.; Handy, N. C. *Chem. Phys. Lett.* **2004**, *393*, 51.
- (33) Hehre, W. J.; Radom, L.; Schleyer, P. V. R.; Pople, J. A. Wiley: New York, 1986.
- (34) Chai, J. D.; Head-Gordon, M. *Phys. Chem. Chem. Phys.* **2008**, *10*, 6615.
- (35) Zhao, Y.; Truhlar, D. G. *Theor. Chem. Acc.* **2008**, *120*, 215.
- (36) Becke, A. D. *J. Chem. Phys.* **1993**, *98*, 5648.
- (37) Perdew, J. P.; Burke, K.; Wang, Y. *Phys. Rev. B* **1996**, *54*, 16533.
- (38) Barone, V.; Cossi, M. *J. Phys. Chem. A* **1998**, *102*, 1995.
- (39) Cossi, M.; Rega, N.; Scalmani, G.; Barone, V. *J. Comput. Chem.* **2003**, *24*, 669.
- (40) Himo, F. *Theor. Chem. Acc.* **2006**, *116*, 232.
- (41) Wiberg, K. B. *Tetrahedron* **1968**, *24*, 1083.
- (42) Reed, A. E.; Curtiss, L. A.; Weinhold, F. *Chem. Rev.* **1988**, *88*, 899.
- (43) Glendening, E. D.; Reed, A. E.; Carpenter, J. E.; Weinhold, F. Theoretical Chemistry Institute, University of Wisconsin.
- (44) Osakabe, T.; Fujii, Y.; Hata, M.; Tsuda, M.; Neya, S.; Hoshino, T. *Chem-Bio Inf. J.* **2004**, *4*, 73.
- (45) Cysewski, P.; Bira, D.; Bialkowski, K. *J. Mol. Struct.: THEOCHEM* **2004**, *678*, 77.
- (46) Doi, M.; In, Y.; Kikuchi, M.; Ishida, T.; Inoue, M. *J. Chem. Soc., Perkin Trans. 1* **1991**, 55.
- (47) Jang, Y. H.; Goddard, W. A.; Noyes, K. T.; Sowers, L. C.; Hwang, S.; Chung, D. S. *Chem. Res. Toxicol.* **2002**, *15*, 1023.
- (48) Davies, M. W.; Clarke, A. J.; Clarkson, G. J.; Shipman, M.; Tucker, J. H. R. *Chem. Commun.* **2007**, 5078.
- (49) Bialkowski, K.; Cysewski, P.; Olinski, R. Z. *Naturforsch., C* **1996**, *51*, 119.
- (50) Banerjee, A.; Yang, W.; Karplus, M.; Verdine, G. L. *Nature* **2005**, *434*, 612.